

In Situ Electrochemical Testing of Uranium Dioxide under Anoxic Conditions

FY19 Report

September 2019

Edgar C. Buck
Xiao-Ying Yu
Jenn Yao
Dallas D. Reilly
Jiyoung Son
Sayan D. Chatterjee
Bruce K. McNamara
Cyrena A. Parker
Eugene S. Ilton

DISCLAIMER

This report was prepared as an account of work sponsored by an agency of the United States Government. Neither the United States Government nor any agency thereof, nor Battelle Memorial Institute, nor any of their employees, **makes any warranty, express or implied, or assumes any legal liability or responsibility for the accuracy, completeness, or usefulness of any information, apparatus, product, or process disclosed, or represents that its use would not infringe privately owned rights.** Reference herein to any specific commercial product, process, or service by trade name, trademark, manufacturer, or otherwise does not necessarily constitute or imply its endorsement, recommendation, or favoring by the United States Government or any agency thereof, or Battelle Memorial Institute. The views and opinions of authors expressed herein do not necessarily state or reflect those of the United States Government or any agency thereof.

PACIFIC NORTHWEST NATIONAL LABORATORY
operated by
BATTELLE
for the
UNITED STATES DEPARTMENT OF ENERGY
under Contract DE-AC05-76RL01830

Printed in the United States of America

Available to DOE and DOE contractors from
the Office of Scientific and Technical
Information,
P.O. Box 62, Oak Ridge, TN 37831-0062
www.osti.gov
ph: (865) 576-8401
fox: (865) 576-5728
email: reports@osti.gov

Available to the public from the National Technical Information Service
5301 Shawnee Rd., Alexandria, VA 22312
ph: (800) 553-NTIS (6847)
or (703) 605-6000
email: info@ntis.gov
Online ordering: <http://www.ntis.gov>

In Situ Electrochemical Testing of Uranium Dioxide under Anoxic Conditions

FY19 Report

September 2019

Edgar C. Buck
Xiao-Ying Yu
Jenn Yao
Dallas D. Reilly
Jiyoung Son
Sayan D. Chatterjee
Bruce K. McNamara
Cyrena A. Parker
Eugene S. Ilton

Prepared for
the U.S. Department of Energy
under Contract DE-AC05-76RL01830

Pacific Northwest National Laboratory
Richland, Washington 99354

Abstract

Prediction of the corrosion behavior of spent uranium oxide (UO₂) fuel is needed for developing predictive performance assessment models for a geologic repository. Currently, the Fuel Matrix Dissolution Model (FMDM) is being used for modeling UO₂ chemistry in the Engineered Barrier System (EBS) and includes the effects of oxidants, oxygen and hydrogen peroxide generated from radiolysis of the fuel in contact with water as well as the role of hydrogen on limiting corrosion.

The aim of this work is to investigate the corrosion of UO₂ *in-situ* in the Scanning Electron Microscope (SEM). The corrosion potential (E_{corr}) is measured using an electrochemical workstation and a unique microfluidic reactor containing three-electrodes and compatible for multiple analytical platforms, termed System for Analysis at the Vacuum Liquid Interface (SALVI) electrochemical cell (E-cell) which has been developed at PNNL. This approach aims to provide real-time and *in operando* monitoring of UO₂ electrode stability and morphological change and to study the UO₂ corrosion process at the microscale. The results will be utilized to support the Mixed Potential Model (MPM) that has been developed for the repository program.

Summary

Work this year has involved establishing the capabilities to perform in situ electrochemical corrosion testing of uranium dioxide (UO₂) in the electron microscopy. Equipment for performing this type of work was purchased and built. An in situ Linkham (McCrone Associates, Westmount, IL) THMS 600 liquid stage for conducting corrosion experiments was purchased as well as an EHI 660 E (CH Instruments, Inc., Austin, TX) electrochemical workstation. Equipment for building electron microscope capable testing cells including a PIE Scientific (Union City, CA) Tergo™ Plasma Cleaner and low temperature oven were also obtained and a specialized chamber for preparing the *in-situ* cells in a clean environment. Furthermore, we purchased a vacuum capable feedthrough port from ThermoFisher, Inc. (Hillsboro, OR) that replaced an existing port on the FEI Quanta 250FEG Scanning Electron Microscope (SEM) and would allow the electrical lines from the Echem workstation into the *in-situ* cell once inside the electron microscope. Additional staff that were experts on electrochemistry and the operation of the *in-situ* cells were brought onto the project.

Characterization of nuclear materials in solid particles or particles in liquid slurry, particularly in high level waste, can establish the elemental, organic, and isotopic compositions that effect the properties of the materials during nuclear fuel cycle activities and processes. Techniques to evaluate such detailed information, even at small concentrations, can support nuclear materials and science programs by increasing our ability to manage and control nuclear materials. However, radioactive materials analysis in liquids and slurries can be challenging using bulk approaches. We have developed a vacuum compatible microfluidic interface, system for analysis at the liquid vacuum interface (SALVI), to enable surface analysis of liquids and liquid-solid interactions using scanning electron microscopy (SEM) and time-of-flight secondary ion mass spectrometry (ToF-SIMS). In this work, we illustrate the initial results from the analysis of liquid samples of importance in the geologic disposal of UO₂ spent nuclear fuel in a repository environment using in situ liquid SEM and SIMS. Our results demonstrate that multimodal analysis of UO₂ materials is possible using SALVI and in situ chemical imaging. Both in situ liquid SEM and SIMS can be used as new approaches to analyze radioactive materials in liquid and slurry forms of high-level nuclear wastes. In addition, stainless materials used in the repository setting from LANL were analyzed using multiple surface tools including SEM, TEM, XPS, and ToF-SIMS. Our results show that material interfaces change as a result of redox chemistry in the repository environment. Further investigation is warranted to understand the physical and chemical processes to support the process model development.

Acknowledgments

ECB thanks RPL Management for access to the Radiological Microscopy Suite (RMS) at PNNL and for the modification of existing instruments for conducting these experiments and access to the JEOL GrandARM Scanning Transmission Electron Microscope. XYY and JY thank the support of the Pacific Northwest National Laboratory TOP program for the support to obtain the initial in situ liquid SIMS results of uranium samples. The programmatic support of this work is from the DOE Nuclear Energy Spent Fuel Waste Science Technology (SFWST) program. Pacific Northwest National Laboratory is operated by Battelle under the contract DE-AC05-76RL01830.

Acronyms and Abbreviations

2D	Two Dimensional
3D	Three Dimensional
BSE	Backscattered Electron Imaging
CBED	Convergent Beam Electron Diffraction
CE	Counter Electrode
DRIE	Deep Reactive Ion Etching
EELS	Electron Energy Loss Spectroscopy
EBS	Engineered Barrier System
Echem	Electrochemical
EDS	X-ray energy dispersive spectroscopy
FIB	Focused Ion Beam
FMDM	Fuel Matrix Dissolution Model
KOH	Potassium Hydroxide
LANL	Los Alamos National Laboratory
MPM	Mixed Potential Model
PDMS	Polydimethylsiloxane
PNNL	Pacific Northwest National Laboratory
RE	Reference Electrode
RM	Radiolysis Model
SALVI	System for Analysis at the Liquid Vacuum Interface
SE	Secondary Electron Imaging
SEM	Scanning Electron Microscopy
SIMS	Secondary Ion Mass Spectrometry
SNF	Spent Nuclear Fuel
STEM	Scanning Transmission Electron Microscopy
ToF-SIMS	Time of Flight SIMS
WE	Working Electrode

Contents

Abstract.....	ii
Summary	iii
Acknowledgments.....	iv
Acronyms and Abbreviations.....	v
Contents	vi
Tables ix	
1.0 Introduction	1
1.1 The SALVI Cell	1
2.0 Experimental Setup	3
2.1 Adapting UO ₂ as a Working Electrode in the SALVI E-cell	3
2.1.1 Development of the Electrode	3
2.1.2 Next step for the fabrication of the micrometer gold electrode	5
2.2 <i>In Situ</i> Liquid ToF-SIMS	5
2.3 In Situ Liquid SEM Using the Existing SALVI E-Cell.....	6
2.4 Electrochemistry Analysis of Liquid Sample Containing Uranium.....	7
2.5 Multimodal Analysis on LANL's Corrosion Sample.....	8
2.6 Sample Preparation	9
2.6.1 Liquid Samples Analyzed Using In Situ Liquid SIMS	9
2.6.2 Liquid Samples Analyzed Using the Electrochemistry Workstation	9
2.6.3 LANL Metal Coupon Preparation.....	9
3.0 RESULTS AND DISCUSSIONS	11
3.1 In Situ Liquid SIMS of UO ₂	11
3.2 Electrochemical Analysis of Uranyl Nitrate for In Situ SEM	12
3.3 Multimodal Imaging of the LANL Metal Coupon	13
4.0 CONCLUSIONS	19
5.0 References.....	20

Figures

Figure 1. (A) The vacuum compatible SAVLI device; (B) SALVI installed on the SEM stage in the Quanta SEM (C); D) SALVI installed on the ToF-SIMS stage before loading to the loadlock in the IONTOF ToF-SIMS V instrument (E).	2
Figure 2. The schematic of the gold substrate on the SiN membrane window.....	3
Figure 3. The microelectrode features using shadow masking: (A) ~400 μm X 400 μm and (B) ~500 μm X 500 μm	4
Figure 4. The schematic showing electrode fabrication using wet etching on a SiN membrane window	5
Figure 5. (A) The vacuum compatible SAVLI device mounted on sample holder before ToF-SIMS analysis; (B) Secondary ion image of SALVI's microchannel being punched through by Bi_3^+ ion beam; and (C) SALVI's microchannel viewed under microscope for locating the analysis area.....	6
Figure 6. (A) In operando SEM setup showing the SALVI E-cell (insert) connected with an electrochemical station; and (B) cyclic voltammograms acquired using this setup.....	7
Figure 7. SALVI E-cell with uranium containing electrolyte in an ambient environment	8
Figure 8. (A) Complete metal coupon as received, (B) trimmed smaller pieces and a piece polished and fixed in the epoxy, and (C) sample coupons mounted in the ToF-SIMS sample holder.....	10
Figure 9. Mass spectra comparison of liquid samples analyzed using liquid SIMS	11
Figure 10. Comparison of normalized 2D images of UO_2^+ and $\text{C}_4\text{H}_5\text{N}_2^+$ among three liquid samples	12
Figure 11. (A) Cyclic voltammogram of 0.1 M HNO_3 and (B) 1mM uranyl nitrate in 0.1 M HNO_3	13
Figure 12. Positive ions detected from coupon interface fixed in epoxy.....	14
Figure 13. 2D images resulting from SIMS imaging technique capture the distribution of the dominant elements and molecules on the clay, clay-interface and stainless steel surface	15
Figure 14. Depth profiling analysis of clay surface of metal coupon	16

- Figure 15. 3D visualization of Al^+ and Fe^+ distributions from the black (A) and gray area (B) in the stainless steel coupon..... 16
- Figure 16. Image and diffraction patterns of the corrosion rind with an EDS line profile and elemental maps. The oxide layer contained particles of Ni-sulfide. Both Fe and Cu were present in the oxide layer; but, at lower levels than in the metal. Whereas, Cr was uniform throughout the corrosion rind. The clay was a sodium alumino-silicate. 17
- Figure 17. (A) Image of the corrosion rind, (B) EELS elemental maps of the major elements, and (C) EELS spectra of three major regions noted in (A), including a Fe-Ni particle in the clay, most likely a sulfide. Shift in the Fe- $L_{2,3}$ edge indicates oxidation of Fe in the clay relative to the other phase. 18

Tables

Table 1. Peak identification of species detected from the corrosion interface	14
---	----

1.0 Introduction

In a reducing or anoxic environment, the oxidation of uranium dioxide (UO_2) spent nuclear fuel can only occur from the production of oxidants from radiolysis of contacting water in the Engineered Barrier System (EBS) of the geologic repository. Within the SFWST program, a model that captures the role of oxidant production is termed the Radiolysis Model (RM). The EBS environment, however, is expected to limit oxidation through the production of H_2 gas from anoxic corrosion of iron. These processes have been described in a Mixed Potential Model (MPM) or Fuel Matrix Dissolution Model (FMDM) from modeling the corrosion rate of spent fuel that combines the RM sub-model with an electrochemical corrosion model (Buck and Wittman 2014, Jerden Jr, Frey et al. 2015). The EBS that contains other components may result in more complex processes also occurring (Caporuscio, Palaich et al. 2017). Previous, experimental validation of the corrosion model under oxidizing conditions has used flow through experiments but these would be inadequate to describe the processes that might occur under anoxic conditions. To validate the FMDM, it is necessary to obtain measurements of the values predicted by the model, namely, the electrochemical corrosion potential. Besides using macroscale approaches to study the multiphase chemistry, it is important to probe the interfacial phenomena at the solid-liquid interface directly using novel chemical imaging approaches. Of particular relevance to the new approach presented in this report, a commercial in situ liquid cell was recently used to study the electron beam induced radiolysis of UO_2 particles in solution (Buck, Wittman et al. 2018) and the dissolution of boehmite (Conroy, Soltis et al. 2017). A vacuum-compatible and transferrable microfluidic reactor, namely System for Analysis at the Liquid Vacuum Interface (SALVI), was invented at the Pacific Northwest National Laboratory (PNNL) and it has enabled in situ liquid scanning electron microscopy (SEM) (Yang, Yu et al. 2011, Yang, Zhu et al. 2014) and in situ liquid time-of-flight secondary ion mass spectrometry (ToF-SIMS) (Yang, Yu et al. 2011, Yu, Yu et al. 2017). Compared to the existing wet cell SEM approaches, (Thiberge, Zik et al. 2004, Nishiyama, Suga et al. 2010), the liquid surface is probed directly by the primary electron beam, because the microfluidic cell is partially open to vacuum with micrometer-sized apertures. In addition, the beam effect and memory effect can be minimized by flowing the liquid (Yang, Yu et al. 2011, Yang, Zhu et al. 2014). This technique has provided an unique in situ chemical mapping approach for investigating challenging solid-liquid, air-liquid, and liquid-liquid interfaces, as illustrated by Ding et al., Sui et al., and Yu et al. (Ding, Zhou et al. 2016, Sui, Zhou et al. 2017, Yu, Yao et al. 2018). This multi-modal imaging tool could also be used to study materials relevant to geological disposal where we are interested in several complex interfacial processes. We started studies with two model systems, UO_2 and iron oxide (Fe_3O_4) in water to demonstrate feasibility and to develop the capabilities to perform this for spent fuel. These two systems also represent the major chemical components described in the FMDM for the EBS.

1.1 The SALVI Cell

The vacuum compatible microfluidic device, termed SALVI was developed at PNNL by Yu and co-workers (Yang, X.-Y. et al. 2011, Yu, Yang et al. 2011, Yu, Liu et al. 2013). The design details have been provided in many other papers and a version of SALVI is now available commercially as Wet Cell II Liquid Probe System marketed by Structure Probe, Inc. (West Chester, PA). A polydimethylsiloxane (PDMS) block with a 100-500 μm wide by 300 μm deep channel was bonded with a 50 nm thick SiN membrane after oxygen plasma treatment. Approximately 10 μL of the analyte liquid mixture was injected into SALVI via its

polytetrafluoroethylene tubing and sealed by polyether ether ketone union afterwards. A photo of a SALVI device is shown in **Error! Reference source not found.A**. Figure 1B shows the SALVI device installed in the SEM stage prior to in situ liquid SEM analysis. Figure 1C shows the port on the SEM instrument where the electrochemical workstation feedthrough is installed. Figure 1D depicts the SALVI device mounted on the ToF-SIMS stage prior to shuttling into the main chamber. Figure 1E depicts the relative location of the main chamber and where the SALVI is located during analysis (Yu, Yao et al. 2019).

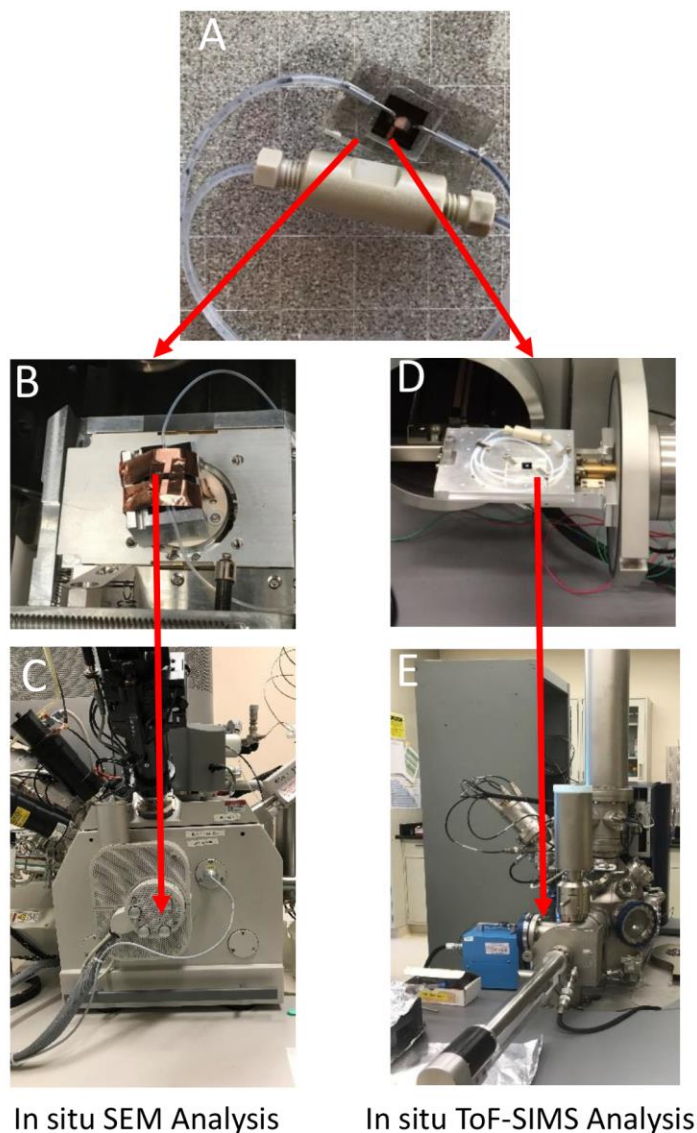


Figure 1. (A) The vacuum compatible SAVLI device; (B) SALVI installed on the SEM stage in the Quanta SEM (C); D) SALVI installed on the ToF-SIMS stage before loading to the load lock in the IONTOF ToF-SIMS V instrument (E).

2.0 Experimental Setup

2.1 Adapting UO_2 as a Working Electrode in the SALVI E-cell

2.1.1 Development of the Electrode

One of the key developments to study the UO_2 electrochemistry in operando is to integrate UO_2 as the working electrode (WE) in the SALVI E-cell. We started by using the gold (Au) WE sputter coated on the silicon nitride (SiN) membrane as a conductive layer and substrate for the UO_2 to attach to. The source of UO_2 is from environmental barrier. The UO_2 piece for the microanalysis is limited by the SEM-FIB. The maximal size of UO_2 is estimated to be approximately $10\ \mu\text{m}$ to $20\ \mu\text{m}$. We select microfabrication processes based on following three principles: 1) the footprint dimension should be around 1:1 ratio of the target UO_2 WE which is $\sim 10\ \mu\text{m} \times 10\ \mu\text{m}$ and no more than $20\ \mu\text{m} \times 20\ \mu\text{m}$; 2) Microfabrication methods are required for the precision required by the UO_2 electrode size in tens of micrometers; and 3) The performance of the UO_2 WE should be verified and compared against bulk experiments. The reference electrode (RE) and counter electrode (CE) are the same as our existing E-cell devices using other materials. Platinum (Pt) is used for both RE and CE. Slight potential shift is expected when using Pt as RE compared to bulk experiments as demonstrated in previous experiments. However, this slight device performance difference does not affect the investigation of the electrochemistry (Liu, Yu et al. 2014, Yu, Zhou et al. 2016).

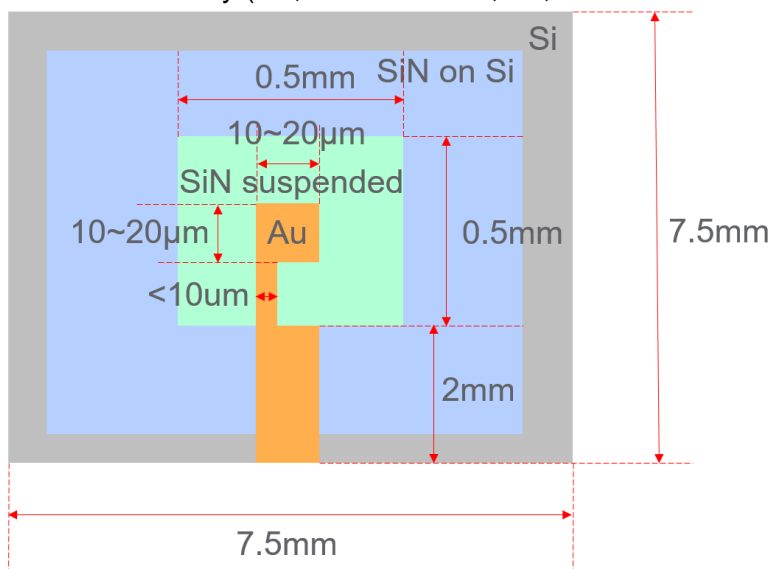


Figure 2. The schematic of the gold substrate on the SiN membrane window

The dimension of the UO_2 WE is estimated to be approximately $10\ \mu\text{m} \times 10\ \mu\text{m}$ and less than $20\ \mu\text{m} \times 20\ \mu\text{m}$. In order to minimize interference from the Au substrate that also can function as a WE when potential is applied, the Au substrate should be just slightly bigger or almost the same size as the UO_2 liftout. The Au substrate film is fabricated on the SiN membrane (Figure 2). The Au substrate is designed to be in the center of the SiN membrane with a dimension of $0.5\ \text{mm} \times 0.5\ \text{mm}$, and the electric connection structure with a dimension of $\sim 500\ \mu\text{m} \times 2\ \text{mm}$ is placed on the edge of the SiN window (Figure 2) for external wire connection.

Since the Au substrate requires micrometer level precision, we utilized microfabrication processes including shadow masking and photolithography. To test feasibility, first we made several of Cr structure prototypes by shadow masking to mimic the effect prior to using Au. The shadow mask was fabricated by photolithography dry etching (DRIE, Oxford-100) and wet etching (KOH). A fabricated shadow mask had several electrode shape holes. Individual SiN chips could be attached one side to the shadow mask before sputtering the metal layer (Denton sputter coater) resulting in the electric conductive substrate layer with the desired features once removing the mask.

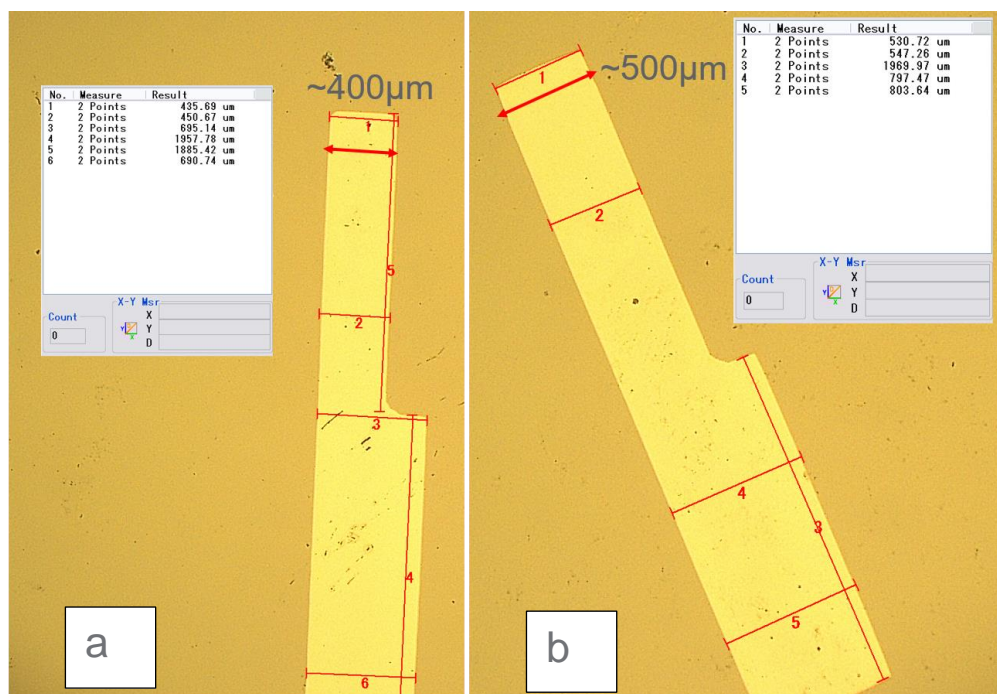


Figure 3. The microelectrode features using shadow masking: (A) $\sim 400 \mu\text{m} \times 400 \mu\text{m}$ and (B) $\sim 500 \mu\text{m} \times 500 \mu\text{m}$.

We first tested $400 \mu\text{m} \times 400 \mu\text{m}$ and $500 \mu\text{m} \times 500 \mu\text{m}$ features with the shadow mask method. With the combination of photolithography dry etching and wet etching, we successfully fabricated a shadow mask contains $400 \mu\text{m} \times 400 \mu\text{m}$ and $500 \mu\text{m} \times 500 \mu\text{m}$ features. Several tested Cr features were sputter coated on the SiN chips shown in Figure 3. Completed Cr test features showed improved features, showing more than 75% size reduction of the footprint (i.e., from $2 \text{ mm} \times 2 \text{ mm}$ to $\sim 450 \mu\text{m} \times 450 \mu\text{m}$). This shows possibility of improvement for making smaller gold electrode substrate.

We then attempted to achieve $15 \mu\text{m} \times 15 \mu\text{m}$ feature with the shadow masking technique. However it was challenging to make fine features using wafer DRIE etching to obtain features in the micrometer level within the $300 \mu\text{m}$ thick wafer, because the actual etching aspect ratio was not close to 1:10 throughout the whole feature. The etched depth of $15 \mu\text{m} \times 15 \mu\text{m}$ was shallower than the $500 \mu\text{m} \times 2 \text{ mm}$ feature used for wire connection, which caused by the uneven etching rate. Therefore, we were not able to achieve the $15 \mu\text{m} \times 15 \mu\text{m}$ feature goal using the shadow mask.

2.1.2 Next step for the fabrication of the micrometer gold electrode

Since shadow mask method was not successful for making $\sim 15 \mu\text{m} \times 15 \mu\text{m}$ features, we plan to apply other microfabrication approaches. Specifically, we will use photolithography to make features directly on premade SiN chips. Figure 4 gives a simple illustration of the etching steps to achieve finer micrometer scale features needed to incorporate the UO_2 WE in the microfluidic E-cell. A layer of platinum will be sputtered as an adhesive layer for the gold layer of $\sim 20 \text{ nm}$ thick. Afterwards, the gold layer will be sputtered on the top the Ti layer for $\sim 40 \text{ nm}$. After sputtering, both metal layers will be etched by wet etching process as depicted in Figure 4. In order to protect the SiN membrane, a layer of photoresist can be used as a protective layer during wet etching of Au and Ti layers. After completion of the fabrication process, the micro-level electrode will be tested by assembling it as the WE using the existing E-cell design.

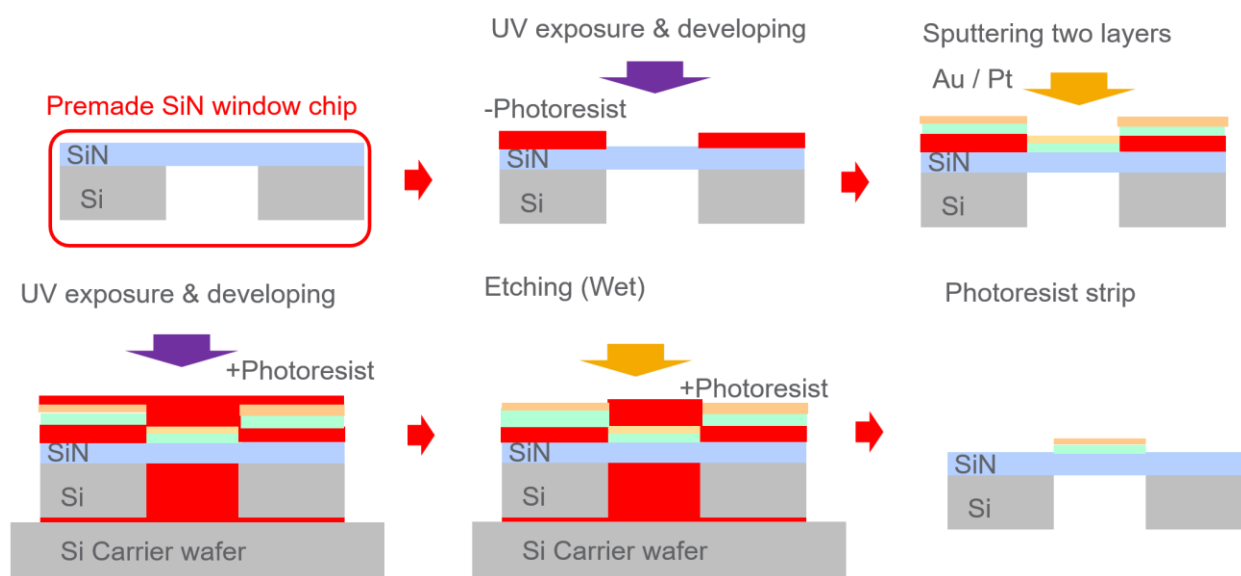


Figure 4. The schematic showing electrode fabrication using wet etching on a SiN membrane window

2.2 In Situ Liquid ToF-SIMS

A TOF-SIMS V spectrometer (IONTOF GmbH, Münster, Germany) was used in this work. The pressure in the main vacuum chamber was maintained below 4×10^{-7} Torr. (Yang, X.-Y. et al. 2011) The SiN window was cleaned by a 1 keV O_2^+ beam to remove surface contamination with a scanning area of $500 \times 500 \mu\text{m}^2$ prior to analysis. An electron flood gun was used to compensate surface charging during analysis. A pulsed 25 keV Bi_3^+ primary ion beam was used with a current $\sim 0.36 \text{ pA}$. The focus spot was about $0.45 \mu\text{m}$ in diameter and the scan area was $2 \mu\text{m}$ in diameter. A pulse width of 150 ns was used to punch through the SiN membrane. (Yu, Zhou et al. 2016) The pulse width was changed to 50 ns to obtain a relatively higher mass resolution in the latter portion of the depth profile. More experimental details have been reported elsewhere (Zhou, Yao et al. 2016, Yu, Yu et al. 2017).

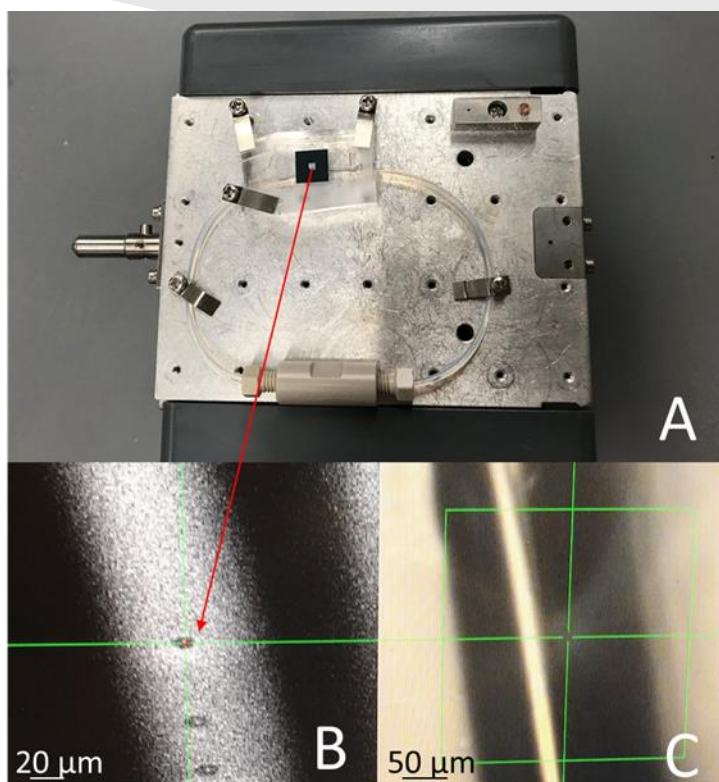


Figure 5. (A) The vacuum compatible SAVLI device mounted on sample holder before ToF-SIMS analysis; (B) Secondary ion image of SALVI's microchannel being punched through by Bi_3^+ ion beam; and (C) SALVI's microchannel viewed under microscope for locating the analysis area.

Figure 5 provides close view of SALVI mounted on the ToF-SIMS's sample holder (Figure 1A) and its microchannel being punched through by Bi_3^+ ion beam (Figure 1B). The microscope imaging was utilized to facilitate locating the analysis area on the SiN window that seals the microchannel. Five holes were drilled through on the SiN window, exposing the liquid sample beneath to the analysis beam. Subsequently, the secondary ions that carry the signature information of the sample were produced. Two samples were measured including 250 ppm uranium in uranium nitrate form dissolved in HNO_3 and laminin solution and control sample containing HNO_3 and laminin only. SALVI is the critical component of in situ liquid SIMS techniques, which enables the liquid samples to be measured directly at microscale. SALVI only requires very minimal liquid sample volume, approximately 30 μL .

2.3 In Situ Liquid SEM Using the Existing SALVI E-Cell

Of particular interest to study the oxidation and reduction of UO_2 , the electrochemical version or the E-cell (Liu, Yu et al. 2014, Yu, Zhou et al. 2016) was used and adapted in this work. The feasibility of using SALVI for in situ characterization of particles in liquid was demonstrated in our previous work (Yao, Arey et al. 2017, Yu, Arey et al. 2019). This paper shows initial results of in operando study of spent fuel relevant systems using the SALVI E-cell. Two FEI Quanta 3D FIB-SEM instruments were used. Both low and high vacuum modes SEM were employed. The radiological material was analyzed in the Quanta 250 FEG SEM housed in the Radiological Processing Laboratory (RPL) at the PNNL. Non-radiological materials were

analyzed to optimize imaging conditions. The iron oxide (Fe_3O_4) in deionized water (DI) mixture was analyzed in the Quanta SEM RPL. A standard operation procedure of in situ liquid SEM was described previously (Yao, Arey et al. 2017, Yu, Arey et al. 2019).

The goal of this work is to conduct in operando SEM of UO_2 simulating the spent fuel conditions. Figure 6 depicts the experimental setup including an electrochemical station connected with a SALVI E-cell. Figure 6b shows a series of cyclic voltammograms obtained with this setup using a standard solution consisting of 2 mM $\text{K}_3\text{Fe}(\text{CN})_6$ and 1 M KNO_3 in DI water. Reagents were acquired from Sigma-Aldrich. This initial result demonstrates the performance of the approach prior to using radiological materials. In operando results and the application of in situ SEM imaging in studying nuclear materials are presented.

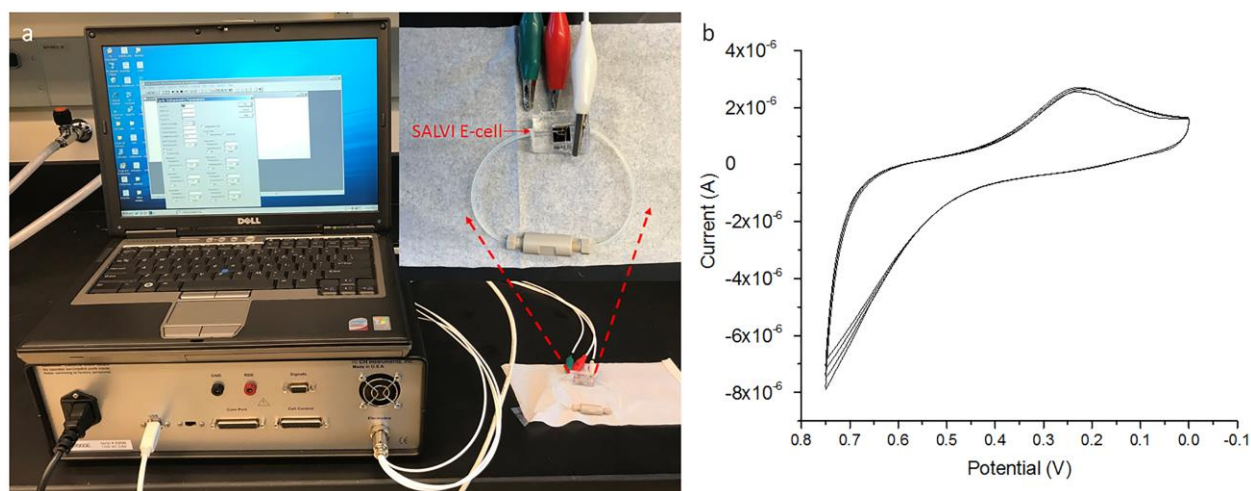


Figure 6. (A) In operando SEM setup showing the SALVI E-cell (insert) connected with an electrochemical station; and (B) cyclic voltammograms acquired using this setup.

2.4 Electrochemistry Analysis of Liquid Sample Containing Uranium

Next, we performed electrochemistry experiments using a uranium containing electrolyte in the SALVI E-cell. An EHI 660 E (CH Instruments, Inc., Austin, TX) electrochemical workstation was used. The E-cell was mounted on the sample stage of the Quanta 250 FEG SEM and was tested in the ambient condition. The three electrodes were connected to the electrochemical workstation via corresponding wires as shown in Figure 7. More results are shown in the Results and Discussion section.

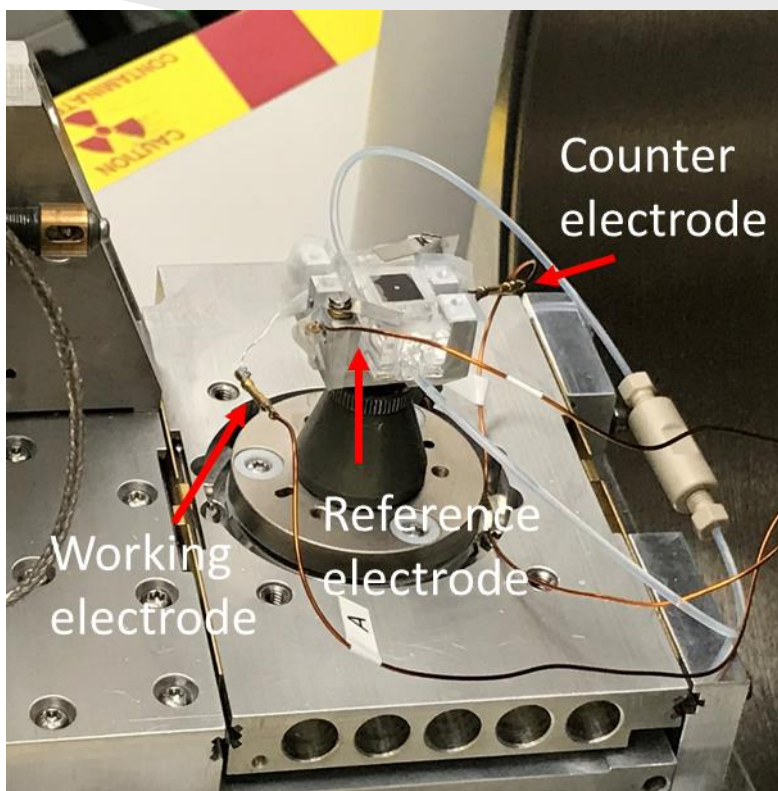


Figure 7. SALVI E-cell with uranium containing electrolyte in an ambient environment

2.5 Multimodal Analysis on LANL's Corrosion Sample

A stainless-steel metal coupon was received from Los Alamos National Laboratory (LANL) to examine the unprocessed Wyoming bentonite and the clay-stainless steel metal interface. Multiple analytical techniques including ToF-SIMS, STEM-EDS, TEM-EELS, and SEM-EDS were used to examine the top surface and cross-sectional interface of the coupon.

In ToF-SIMS analysis, three analysis modes were conducted including high mass resolution mass spectrum, high spatial resolution imaging, and depth profiling. Data were acquired in both positive and negative ion mode. In the mass spectrum mode, 25 KeV Bi_3^+ was sputtered on the $100\ \mu\text{m} \times 100\ \mu\text{m}$ area, collecting the high mass resolution spectra for 60 scans with 128×128 -pixel resolution. In the imaging mode, the same areas were analyzed for 200 scans with 256×256 -pixel resolution. In the depth profiling mode, 25 KeV Bi^+ was applied as the primary analysis beam, coupled with 2 KeV O_2 as the sputter beam to analyze the sample surface layer by layer.

A cross-sectional mount of the metal sample was prepared by polishing to a $0.25\ \mu\text{m}$ finish. The sample was then introduced into a FEI Helios 660 NanoLab™ field emission gun (FEG) dual beam focused gallium ion beam/scanning electron microscope (FIB-SEM) equipped with an EDAX (EDAX Inc., Mahwah, NJ) compositional analysis system. The current and accelerating voltage of the ion beam used for prep was between 9 pA to 9 nA and 2–30 kV, respectively, depending on the progress of the thinning operation. The thinned specimens were attached to Cu-Omniprobe grids.

Lift-out specimens for scanning transmission electron microscopy (STEM) were characterized on a JEOL (Japan) ARM300F (GrandARM) probe-corrected microscope equipped with high angle annular dark field (HAADF) and bright field (BF) detectors, dual Bruker x-ray energy dispersive spectrometers (EDS), and Gatan (Gatan Inc., Pleasanton, CA) Quantum Image Filter for Electron Energy-Loss Spectroscopy (EELS) and imaging. Diffraction patterns were collected on a Gatan 4D STEM system, and EELS data, and electron micrographs were analyzed with Gatan DigitalMicrograph™ 3.0.

2.6 Sample Preparation

Two types of sample preparation were described below. One was for liquid SIMS and liquid SEM and the other stainless-steel coupon from LANL.

2.6.1 Liquid Samples Analyzed Using In Situ Liquid SIMS

The liquid solution containing uranium was prepared from U1010- uranyl nitrate (Crystal, ACS grade) and hexahydrate (Spectrum Chemical Mfg. Corp.). 250 ppm uranyl nitrate was dissolved in ~0.09 M HNO₃ and 1mg/ml laminin (Sigma L2020-1MG) was added to make the testing mixture.

2.6.2 Liquid Samples Analyzed Using the Electrochemistry Workstation

Two liquid samples loaded in SALVI E-cells were analyzed using the electrochemistry workstation, including 1 mM Uranyl Nitrate in 0.1 M HNO₃ and 0.1 M HNO₃ only as the control sample.

2.6.3 LANL Metal Coupon Preparation

The metal coupon received from LANL was unprocessed and non-radioactive. It was cut into smaller pieces for multimodal analysis using various analytical tools. One piece was fixed in the epoxy with the cross-sectional interface exposed for analysis after polishing. This interface piece was analyzed using ToF-SIMS.

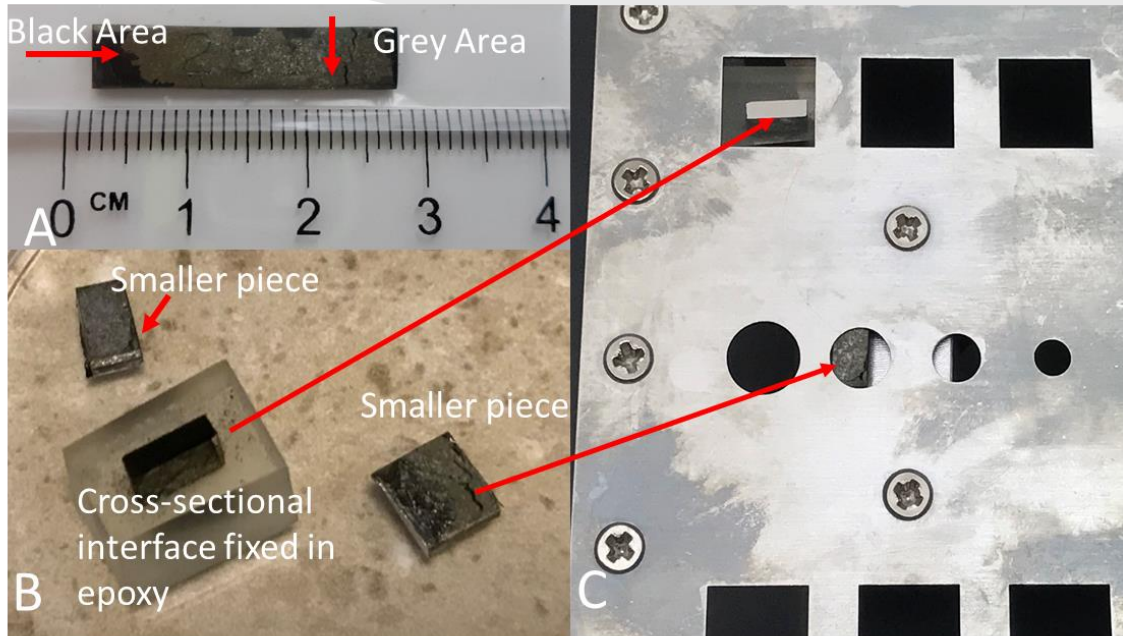


Figure 8. (A) Complete metal coupon as received, (B) trimmed smaller pieces and a piece polished and fixed in the epoxy, and (C) sample coupons mounted in the ToF-SIMS sample holder.

Figure 8A shows photos of the LANL metal coupon as received. Figure 8B gives the pictures of the cross-sectional interface fixed in epoxy resin and one of the small pieces from various analysis. Figure 8C shows how the metal piece was loaded onto the ToF-SIMS stage prior to analysis.

3.0 RESULTS AND DISCUSSIONS

In this section, we will report results from three types of experiments. The first is results from in situ liquid SIMS analysis of UO_2 containing liquid. The second is in situ liquid SEM experiment of uranium containing electrolyte. Third, we will discuss multimodal imaging and analysis of the LANL metal coupon.

3.1 In Situ Liquid SIMS of UO_2

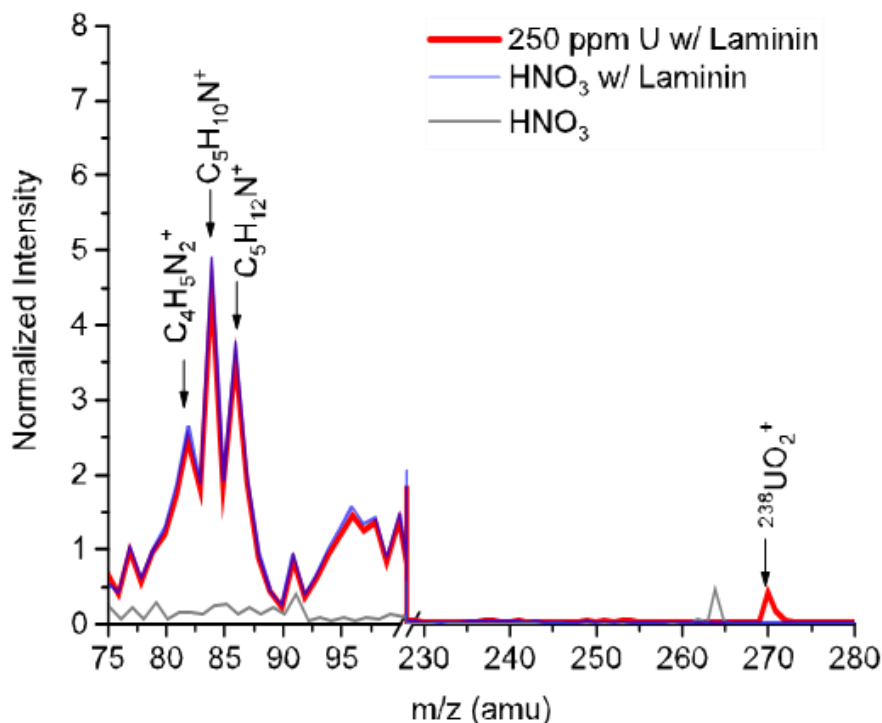


Figure 9. Mass spectra comparison of liquid samples analyzed using liquid SIMS

We conducted in situ liquid SIMS analysis of a liquid mixture containing UO_2 , HNO_3 , and laminin. Although not directly related to the UO_2 spent fuel chemistry, laminin is added to demonstrate the ToF-SIMS capability to identify both organic components and uranium containing compounds. Besides this mixture, we analyzed UO_2 dissolved in nitric acid and nitric acid solution as the control.

The mass spectra acquired from these three liquid samples were normalized to the intensity of NO_2^+ before comparison as seen in Figure 9. The third sample, 3.5% HNO_3 , was presented previously in our last report. The mass spectrum and 2D image from this sample were used for comparison purpose. The high intensities of laminin fragment peaks such as $\text{C}_4\text{H}_5\text{N}_2^+$, $\text{C}_5\text{H}_{10}\text{N}^+$, $\text{C}_5\text{H}_{12}\text{N}^+$ were detected from both samples containing laminin (250 ppm U w/laminin and HNO_3 w/ laminin) but not from the HNO_3 sample as expected. Furthermore, $^{238}\text{UO}_2^+$ was only detected from the uranyl sample, even with the interference of organic species. The normalized 2D image comparisons are presented in Figure 10, confirming the detection of uranium species and organic molecules in the mixture consisting of 250 ppm U and laminin.

Our in-situ liquid SIMS results illustrate that we can use it to detect the changes of UO_2 electrode before and after applying potentials to the electrode and examine the corrosion process of UO_2 . It is envisioned that in situ and in operando approaches will provide new insights into spent fuel chemistry of importance simulating depository conditions and enhance our ability to manage and control nuclear materials at microscale.

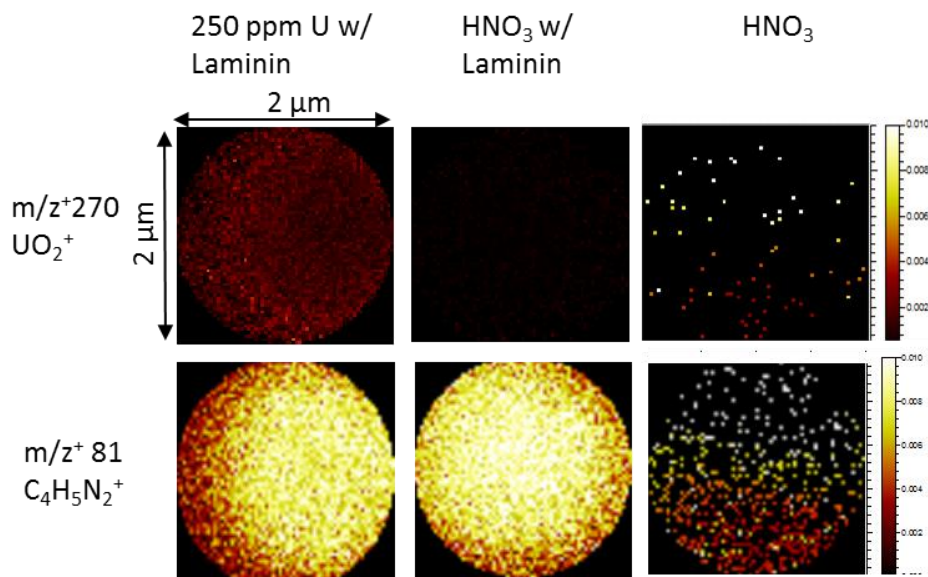


Figure 10. Comparison of normalized 2D images of UO_2^+ and $\text{C}_4\text{H}_5\text{N}_2^+$ among three liquid samples

3.2 Electrochemical Analysis of Uranyl Nitrate for In Situ SEM

The electrochemistry of U (VI) was conducted using a three-electrode SALVI E-cell, with gold film ($\sim 1\text{mm}^2$) as WE, Pt wires as CE and RE, respectively. The cyclic voltammogram of U (VI) nitrate dissolved in 0.1 M HNO_3 showed reduction and possible oxidation processes that were not existing in the control blank sample. The potential process at 0.22 V is assigned to $\text{UO}^+ \rightarrow \text{U}^{4+}$ reduction. The potential process at -0.21 V indicates possible reduction of $\text{U}^{4+} \rightarrow \text{U}^{3+}$, while the process at -0.1V possible oxidation of low valence of U changing to higher valence. (Figure 11). Since WE is gold, the potential of the reduction and oxidation of U may differ slightly from other published report or database using other WE materials (Liu, Yu et al. 2014, Yu, Zhou et al. 2016). In addition, the reduction and oxidation processes that appear in both blank and uranyl nitrate solution may be caused by the Au film, because the effective Au film area is much larger than the UO_2 WE. This result suggest that we use a wider range of potentials in future experiments. In addition, smaller Au film conductive substrate is needed to reduce the interference of H and Au. Future testing will include the scanning rate dependency of the uranyl nitrate using this three-electrode cell with improved UO_2 WE design.

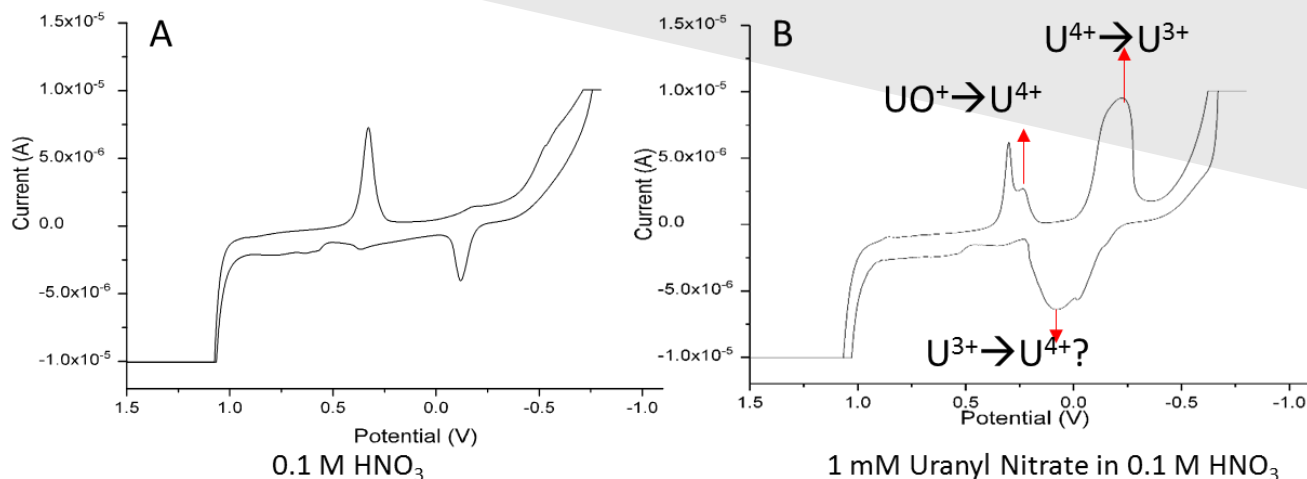


Figure 11. (A) Cyclic voltammogram of 0.1 M HNO_3 and (B) 1mM uranyl nitrate in 0.1 M HNO_3 .

3.3 Multimodal Imaging of the LANL Metal Coupon

We received a sample of corroded metal from F. Caporuscio of LANL. This specimen was cut into sections for further testing and analysis. Extensive characterization by SEM and XRD has been reported by LANL on this specimen (Caporuscio, Cheshire et al. 2014 995). More details of specimen preparation are provided previously.

Figure 12 presents the positive mass spectrum detected from the interface of the metal coupon using high mass resolution mode of ToF-SIMS. The possible identification of the detected peaks are listed in Table 1. Combined with 2D images (Figure 13) of the elemental and molecular information of the interface, our results show the main chemical components of the clay, the clay-metal interface, and stainless steel. Elemental components such as K^+ , Ca^+ , and Na^+ from the water that treated the coupon were observed (Figure 10). The observation of Si^+ and SiO^+ (Figure 12) on the clay layer confirms silica (SiO_2) formation, which was observed using SEM in the earlier LANL's report (Caporuscio, et. al, 2014). It is interesting that Fe^+ and Fe(OH)^+ are present in both the stainless steel and clay layer, and the intensity of Cr^+ at the interface is stronger than that in the bulk stainless steel (Figure 13). This observation provides visualized evidence that Fe-saponite forms at the bentonite – steel interface via oxidative leaching of Fe and Ni producing a chromite $(\text{Cr}_{1.04}\text{Fe}_{0.96})(\text{Fe}_{0.69},\text{Ni}_{0.31})\text{O}_4$ passivation layer on the outer surface of the 316SS plates (Caporuscio, Cheshire et al. 2014 995). The ToF-SIMS spectral results demonstrate that SIMS has enough surface sensitivity to provide useful elemental information as SEM. More importantly, SIMS can provide high resolution 2D chemical maps showing the interfacial elemental and molecular distribution, offering mechanistic insights into the bentonite – steel interfacial processes.

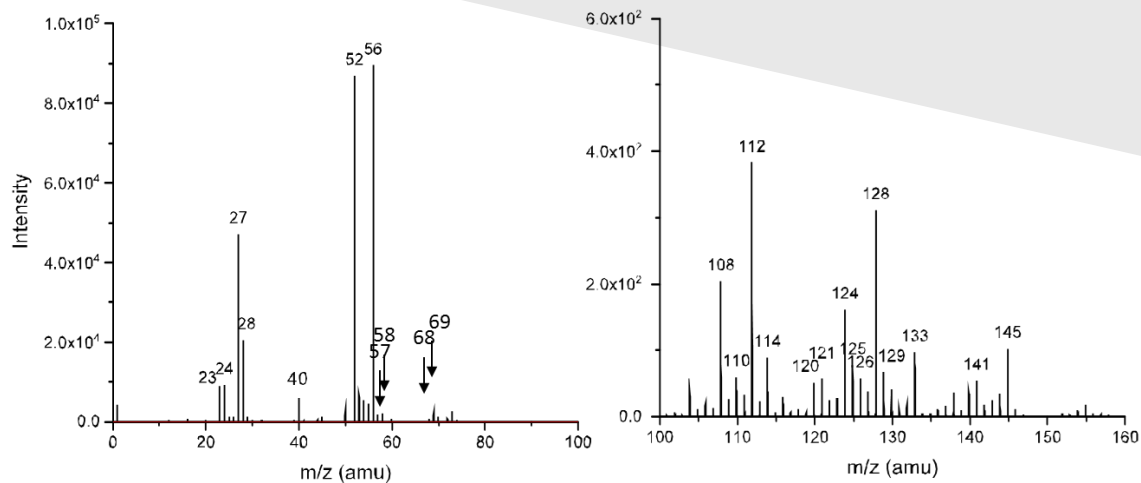


Figure 12. Positive ions detected from coupon interface fixed in epoxy

Table 1. Peak identification of species detected from the corrosion interface

No.	Center Mass (u)	Possible Assignment	No.	Center Mass (u)	Possible Assignment
1	22.99	Na ⁺	8	57.94	Ni ⁺
2	23.98	Mg ⁺	9	67.94	CrO ⁺
3	26.98	Al ⁺	10	68.94	CrOH ⁺
4	27.98	Si ⁺	11	69.95	CrH ₂ O ⁺
5	39.96	Ca ⁺	12	111.88	Fe ₂ ⁺
6	51.94	Cr ⁺	13	128.87	Fe ₂ OH ⁺
7	55.94	Fe ⁺	14	144.86	Fe ₂ O ₂ H ⁺

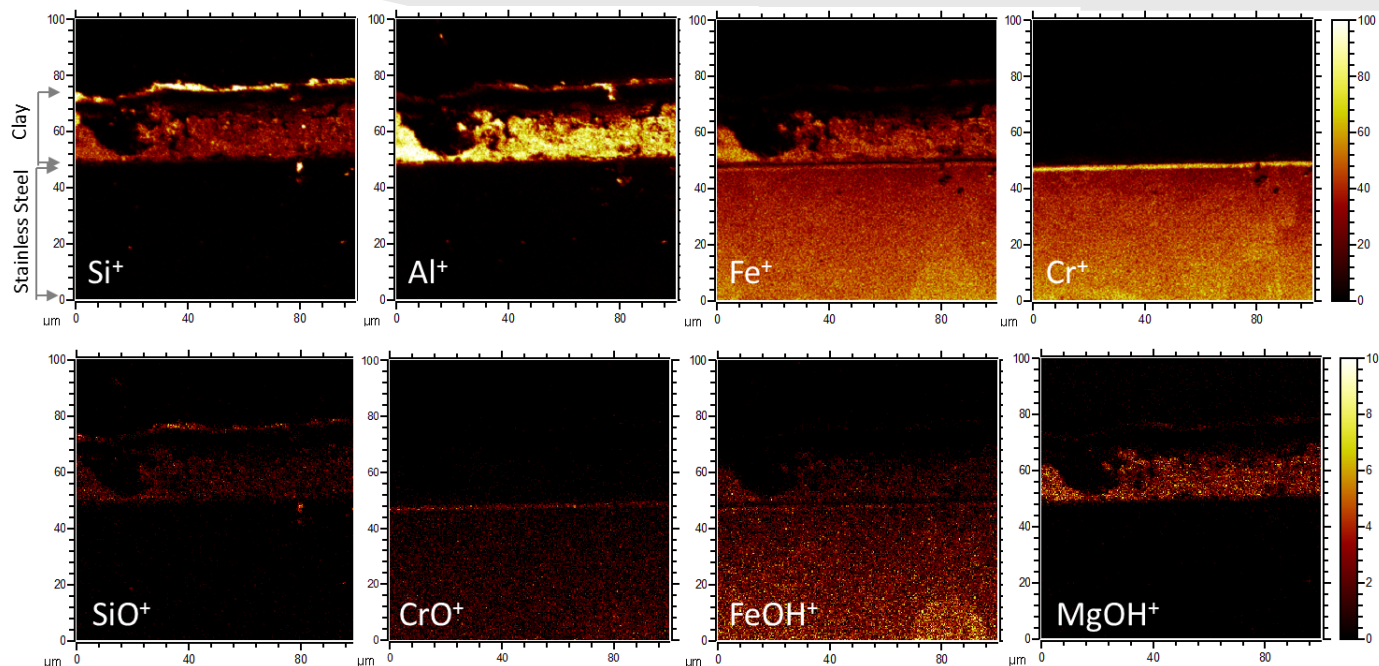


Figure 13. 2D images resulting from SIMS imaging technique capture the distribution of the dominant elements and molecules on the clay, clay-interface and stainless-steel surface

In addition, we use the SIMS depth profiling to reveal the distribution of chemical species in 3D. SIMS depth profiling was applied to the top surface of one of the small pieces. The depth analysis is approximately ~ 800 nm. The chemical species detected are mainly from the clay layer (Figure. 14).

Figure 15 gives two examples of the 3D SIMS analysis from the top surface region of the corroded metal comparing the black and gray areas. Figure 15a shows superimposed 3D images of Al^+ and Fe^+ from the black area. Ions signals from metal are dominant in the black area. Figure 15b shows 3D images Al^+ and Fe^+ from the gray area. Charging causes lower ion intensities compared to the black area. We suspect that iron oxidization was formed on the surface in the gray area.

The 3D SIMS analysis demonstrates the capability of dynamic ToF-SIMS in providing the elemental and molecular information as a function of depth. 3D visualization can be utilized to reveal the species present around the clay-metal interface, providing the insights into the corrosion process at the bentonite - steel interface.

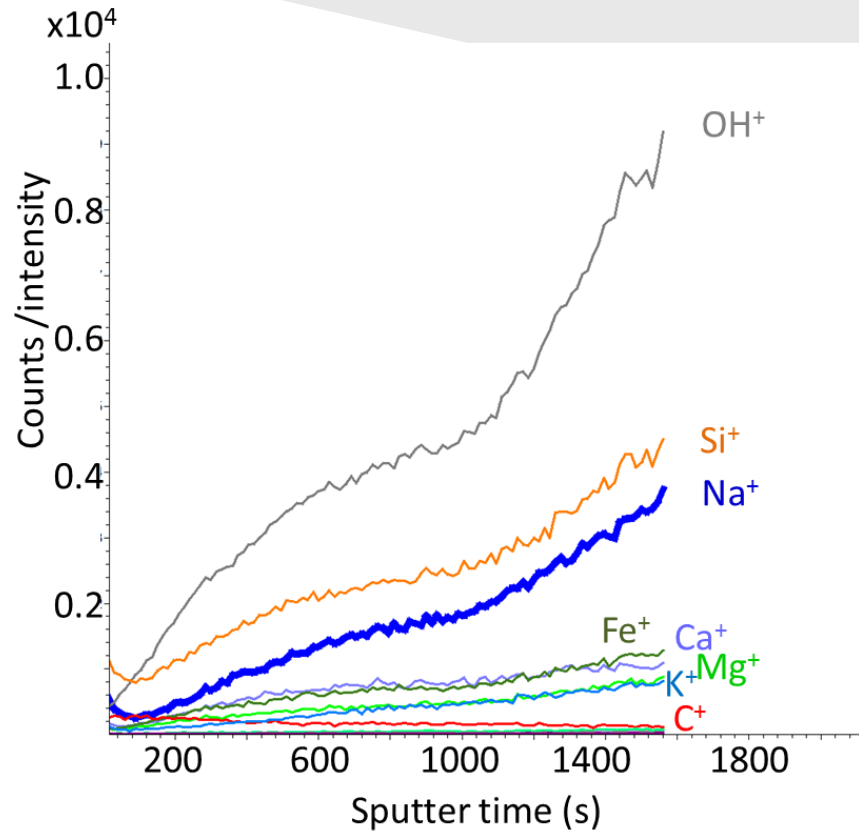


Figure 14. Depth profiling analysis of clay surface of metal coupon

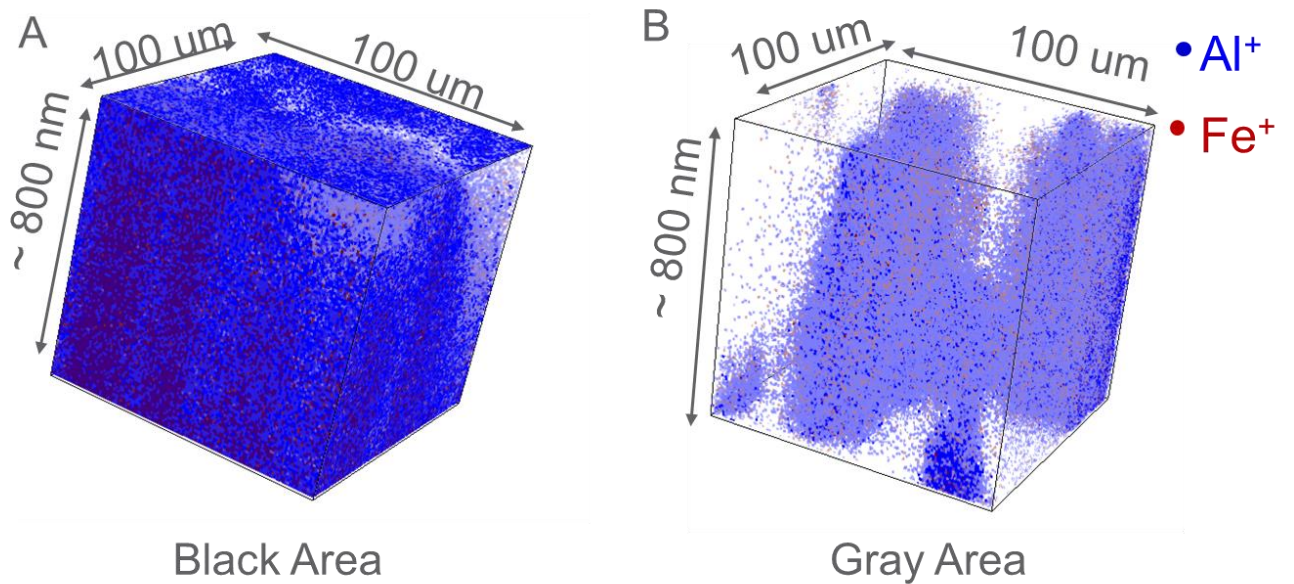


Figure 15. 3D visualization of Al^+ and Fe^+ distributions from the black (A) and gray area (B) in the stainless steel coupon.

Extensive characterization by SEM and XRD has been reported by LANL on this specimen. STEM-EDS and -EELS work was used to understand the mechanism of metal corrosion. The EDS elemental maps show the distribution of elements and the separation of the clay layer from the corroded metal. This is also clearly visible in the STEM image. The clay consists of Na, Al, O, and Si as major components. Other minor elements are also identified but not shown in the figure.

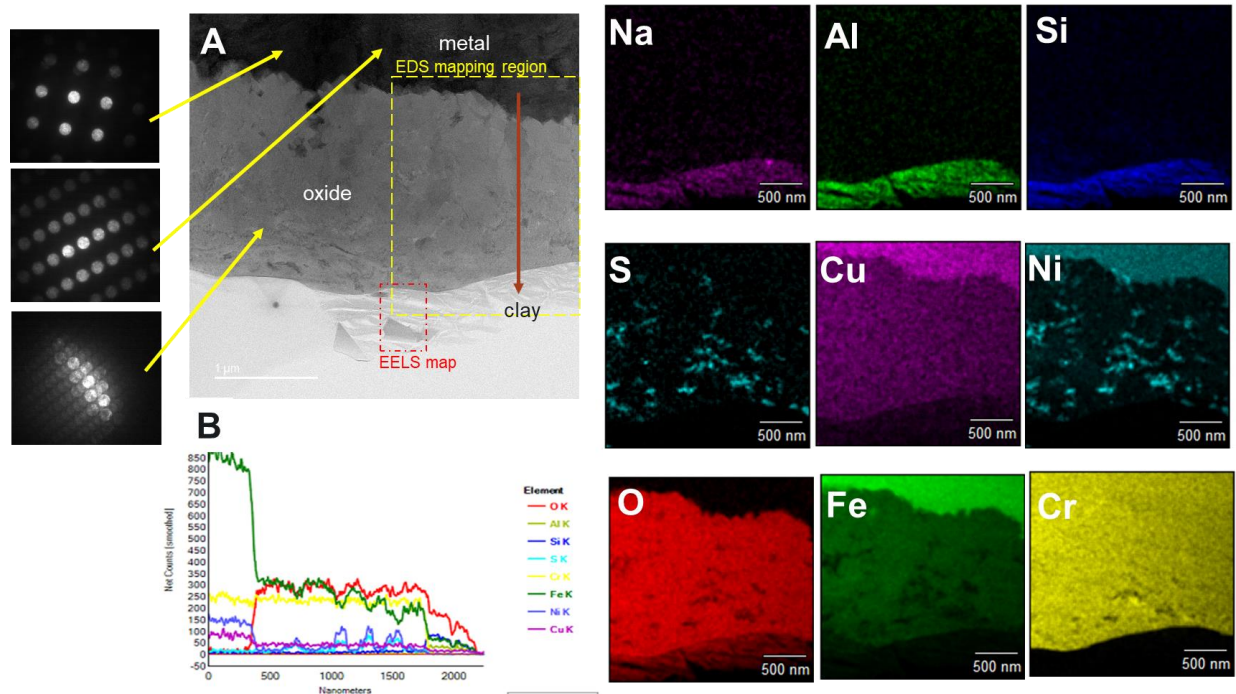


Figure 16. Image and diffraction patterns of the corrosion rind with an EDS line profile and elemental maps. The oxide layer contained particles of Ni-sulfide. Both Fe and Cu were present in the oxide layer; but, at lower levels than in the metal. Whereas, Cr was uniform throughout the corrosion rind. The clay was a sodium aluminosilicate.

Iron is enriched in the metal and present at lower levels in the oxide, as expected. Ni and S have formed sulfides throughout the oxide zone. Diffraction data was also collected from the different regions in the specimen.

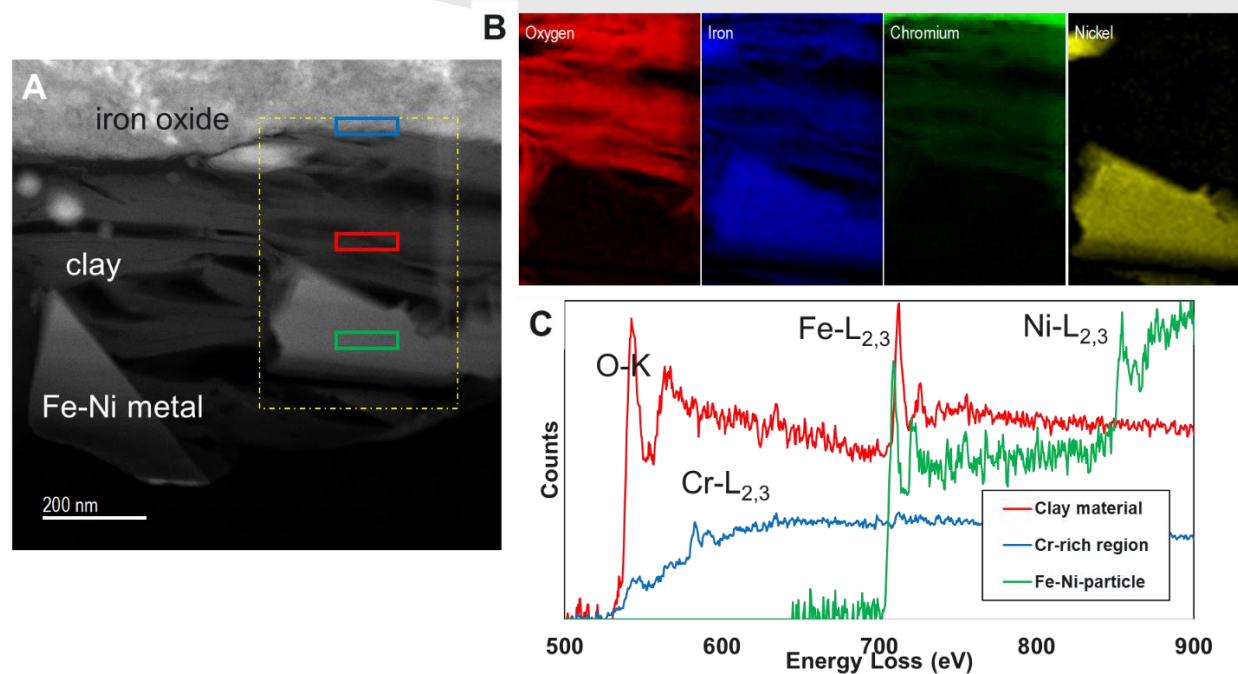


Figure 17. (A) Image of the corrosion rind, (B) EELS elemental maps of the major elements, and (C) EELS spectra of three major regions noted in (A), including a Fe-Ni particle in the clay, most likely a sulfide. Shift in the Fe-L_{2,3} edge indicates oxidation of Fe in the clay relative to the other phase.

4.0 CONCLUSIONS

We are developing the tools that will enable us to conduct in situ liquid SEM analyses of UO_2 to validate the electrochemical model for long-term disposal of nuclear fuel. Furthermore, *in situ* ToF-SIMS analysis could complement the *in-situ* SEM imaging and provide information on the U species forming in solution during the corrosion processes.

5.0 References

- Buck, E. C. and R. S. Wittman (2014). Radiolysis Model Formulation for Integration with the Mixed Potential Model, ; Pacific Northwest National Lab. (PNNL), Richland, WA (United States): Medium: ED; Size: 32 p.
- Buck, E. C., R. S. Wittman, C. Z. Soderquist and B. K. McNamara (2018). "Monitoring bromide effect on radiolytic yields using in situ observations of uranyl oxide precipitation in the electron microscope." RSC Advances **8**(33): 18227-18233.
- Caporuscio, F. A., M. C. Cheshire, M. S. Rearick and C. Jove-Colon (2014). Argillite EBS Experimental Program 2014: Fuel cycle research and development, Los Alamos National Laboratory Sandia National Laboratory.
- Caporuscio, F. A., S. E. M. Palaich, M. C. Cheshire and C. F. Jové Colón (2017). "Corrosion of copper and authigenic sulfide mineral growth in hydrothermal bentonite experiments." Journal of Nuclear Materials **485**: 137-146.
- Conroy, M., J. A. Soltis, R. S. Wittman, F. N. Smith, S. Chatterjee, X. Zhang, E. S. Ilton and E. C. Buck (2017). "Importance of interlayer H bonding structure to the stability of layered minerals." Scientific Reports **7**(1): 13274.
- Ding, Y., Y. Zhou, J. Yao, C. Szymanski, J. Fredrickson, L. Shi, B. Cao, Z. Zhu and X.-Y. Yu (2016). "In Situ Molecular Imaging of the Biofilm and Its Matrix." Analytical Chemistry **88**(22): 11244-11252.
- Jerden Jr, J. L., K. Frey and W. Ebert (2015). "A multiphase interfacial model for the dissolution of spent nuclear fuel." Journal of Nuclear Materials **462**: 135-146.
- Liu, B., X.-Y. Yu, Z. Zhu, X. Hua, L. Yang and Z. Wang (2014). "In situ chemical probing of the electrode-electrolyte interface by ToF-SIMS." Lab on a Chip **14**(5): 855-859.
- Nishiyama, H., M. Suga, T. Ogura, Y. Maruyama, M. Koizumi, K. Mio, S. Kitamura and C. Sato (2010). "Atmospheric scanning electron microscope observes cells and tissues in open medium through silicon nitride film." Journal of Structural Biology **169**(3): 438-449.
- Sui, X., Y. Zhou, F. Zhang, J. Chen, Z. Zhu and X.-Y. Yu (2017). "Deciphering the aqueous chemistry of glyoxal oxidation with hydrogen peroxide using molecular imaging." Physical Chemistry Chemical Physics **19**(31): 20357-20366.
- Thiberge, S., O. Zik and E. Moses (2004). "An apparatus for imaging liquids, cells, and other wet samples in the scanning electron microscopy." Review of Scientific Instruments **75**(7): 2280-2289.
- Yang, L., Y. X.-Y., Z. H. Zhu, T. Thevuthasan and J. P. Cowin (2011). "Making a hybrid microfluidic platform compatible for in situ imaging by vacuum-based techniques." J. Vac. Sci. Technol. A **29**(6): article no. 061101.
- Yang, L., X.-Y. Yu, Z. Zhu, M. J. Iedema and J. P. Cowin (2011). "Probing liquid surfaces under vacuum using SEM and ToF-SIMS." Lab on a Chip **11**(15): 2481-2484.
- Yang, L., Z. Zhu, X.-Y. Yu, E. Rodek, L. Saraf, T. Thevuthasan and J. P. Cowin (2014). "In situ SEM and ToF-SIMS analysis of IgG conjugated gold nanoparticles at aqueous surfaces." **46**(4): 224-228.
- Yao, J., B. W. Arey, L. Yang, F. Zhang, R. Komorek, J. Chun and X.-Y. Yu (2017). "In Situ Characterization of Boehmite Particles in Water Using Liquid SEM." (127): e56058.
- Yu, J., Y. Zhou, X. Hua, Z. Zhu and X.-Y. Yu (2016). "In Situ Characterization of Hydrated Proteins in Water by SALVI and ToF-SIMS." Journal of visualized experiments : JoVE(108): 53708-53708.
- Yu, J., Y. Zhou, X. Hua, Z. Zhu and X.-Y. Yu (2016). "In Situ Characterization of Hydrated Proteins in Water by SALVI and ToF-SIMS." Journal of Visualized Experiments(108): e53708.

- Yu, X.-Y., B. Arey, S. Chatterjee and J. Chun (2019). "Improving in situ liquid SEM imaging of particles." Surface and Interface Analysis **0**(0).
- Yu, X.-Y., B. Liu and L. Yang (2013). "Imaging liquids using microfluidic cells." Microfluidics and Nanofluidics **15**(6): 725-744.
- Yu, X.-Y., L. Yang, J. Cowin, M. Iedema and Z. Zhu (2011). Systems and methods for analyzing liquids under vacuum. uspto.gov. U. S. P. a. T. Office. USA, Battelle Memorial Institute: 16.
- Yu, X.-Y., J. Yao, D. B. Lao, D. J. Heldebrant, Z. Zhu, D. Malhotra, M.-T. Nguyen, V.-A. Glezakou and R. Rousseau (2018). "Mesoscopic Structure Facilitates Rapid CO₂ Transport and Reactivity in CO₂ Capture Solvents." The Journal of Physical Chemistry Letters **9**(19): 5765-5771.
- Yu, X.-Y., J. Yao, Z. Zhu and E. Buck (2019). Analysis of radioactive materials in liquid using in situ SEM and ToF-SIMS. International High-Level Radioactive Waste Management (IHLRWM) Conference, Knoxville, TN, American Nuclear Society.
- Yu, X., J. Yu, Y. Zhou, Y. Zhang, J. Wang, J. E. Evans, X.-Y. Yu, X.-L. Wang and Z. Zhu (2017). "An investigation of the beam damage effect on in situ liquid secondary ion mass spectrometry analysis." **31**(23): 2035-2042.
- Yu, X., J. Yu, Y. Zhou, Y. Zhang, J. Wang, J. E. Evans, X.-Y. Yu, X.-L. Wang and Z. Zhu (2017). "An investigation of the beam damage effect on in situ liquid secondary ion mass spectrometry analysis." Rapid Communications in Mass Spectrometry **31**(23): 2035-2042.
- Zhou, Y., J. Yao, Y. Ding, J. Yu, X. Hua, J. E. Evans, X. Yu, D. B. Lao, D. J. Heldebrant, S. K. Nune, B. Cao, M. E. Bowden, X. Y. Yu, X. L. Wang and Z. Zhu (2016). "Improving the Molecular Ion Signal Intensity for In Situ Liquid SIMS Analysis." J Am Soc Mass Spectrom **27**(12): 2006-2013.